

Supplementary Information

Chemical control of photoinduced charge-transfer direction in a tetrathiafulvalene-fused dipyrrolylquinoxaline difluoroborate dyad

Ping Zhou,^a Ulrich Aschauer,^{*a} Silvio Decurtins,^a Thomas Feurer,^b Robert Häner^a
and Shi-Xia Liu^{*a}

^aDepartment of Chemistry and Biochemistry, University of Bern, Freiestrasse 3, CH-3012 Bern, Switzerland. E-mail: ulrich.aschauer@dcb.unibe.ch; liu@dcb.unibe.ch

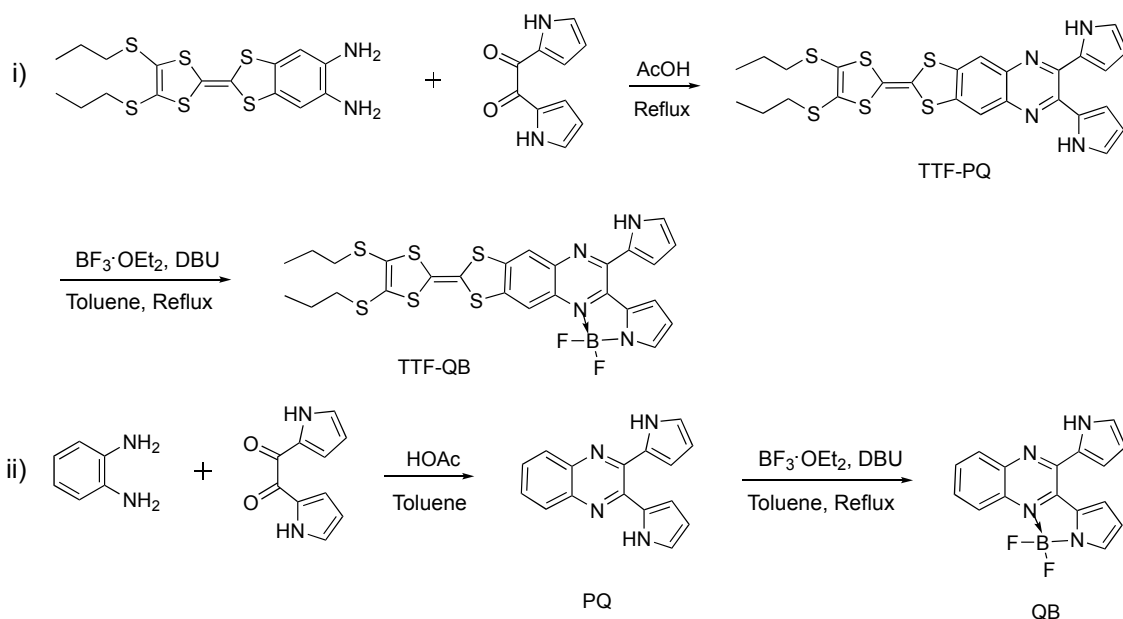
^bInstitute of Applied Physics, University of Bern, Sidlerstrasse 5, CH-3012 Bern, Switzerland.

Experimental Section

General

Air- and/or water-sensitive reactions were conducted under nitrogen and dry, freshly distilled solvents were used. Chemicals used for the synthesis of the compounds were purchased from commercial suppliers (Sigma-Aldrich, TCI or Alfa Aesar). UV-Vis-NIR absorption spectra were recorded on a Perkin Elmer Lambda 900 UV/Vis/NIR spectrometer and UV-vis absorption spectra on a Varian Cary-100 Bio-UV/VIS instrument. ¹H NMR spectra were recorded on a Bruker Avance 300 (300 MHz) spectrometer. Chemical shifts are reported in parts per million (ppm) and are referenced to the residual solvent peak (CD₂Cl₂, δ ¹H = 5.32 ppm). The following abbreviations were used s (singlet), d (doublet), t (triplet) and m (multiplet). Elemental analysis was performed on a Flash 2000 Organic Elemental Analyzer (Thermo Scientific). High resolution mass spectrum (HR-MS) was obtained on a Thermo Fisher LTQ Orbitrap XL using Nano Electrospray Ionization.

Cyclic voltammetry (CV) was performed in a three-electrode cell equipped with a Pt working electrode, a glassy carbon counter-electrode, and Ag/AgCl was used as the reference electrode. The electrochemical experiments were carried out under an oxygen-free atmosphere in dichloromethane with TBAPF₆ (0.1 M) as a supporting electrolyte.



Scheme S1. Synthetic routes for the target TTF-QB and its reference compounds TTF-PQ, PQ and QB.

Synthesis of TTF-PQ. The compound was prepared according to the modified literature procedure.¹ A mixture of 5,6-diamino-2-(4,5-bis(propylthio)-1,3-dithio-2-ylidene)benzo[*d*]-1,3-dithiole (135 mg, 0.3 mmol) and 1,2-di(1*H*-2-pyrrolyl)ethane-1,2-dione (58.5 mg, 0.3 mmol) in glacial acetic acid (30 mL) was heated at 120 °C for 3 h under nitrogen. The solvent was removed under vacuum and the crude product was purified by column chromatography on silica gel eluting with dichloromethane to give the compound TTF-PQ (91 mg, 52%) as a purple-red solid. ¹H NMR δ 9.63 (s, 2H), 7.71 (s, 2H), 7.02-7.00 (m, 2H), 6.92 – 6.89 (m, 2H), 6.27-6.24 (m, 2H), 2.83 (t, *J* = 7.2 Hz, 4H), 1.79-1.62 (m, 4H), 1.02 (t, *J* = 7.3 Hz, 6H).

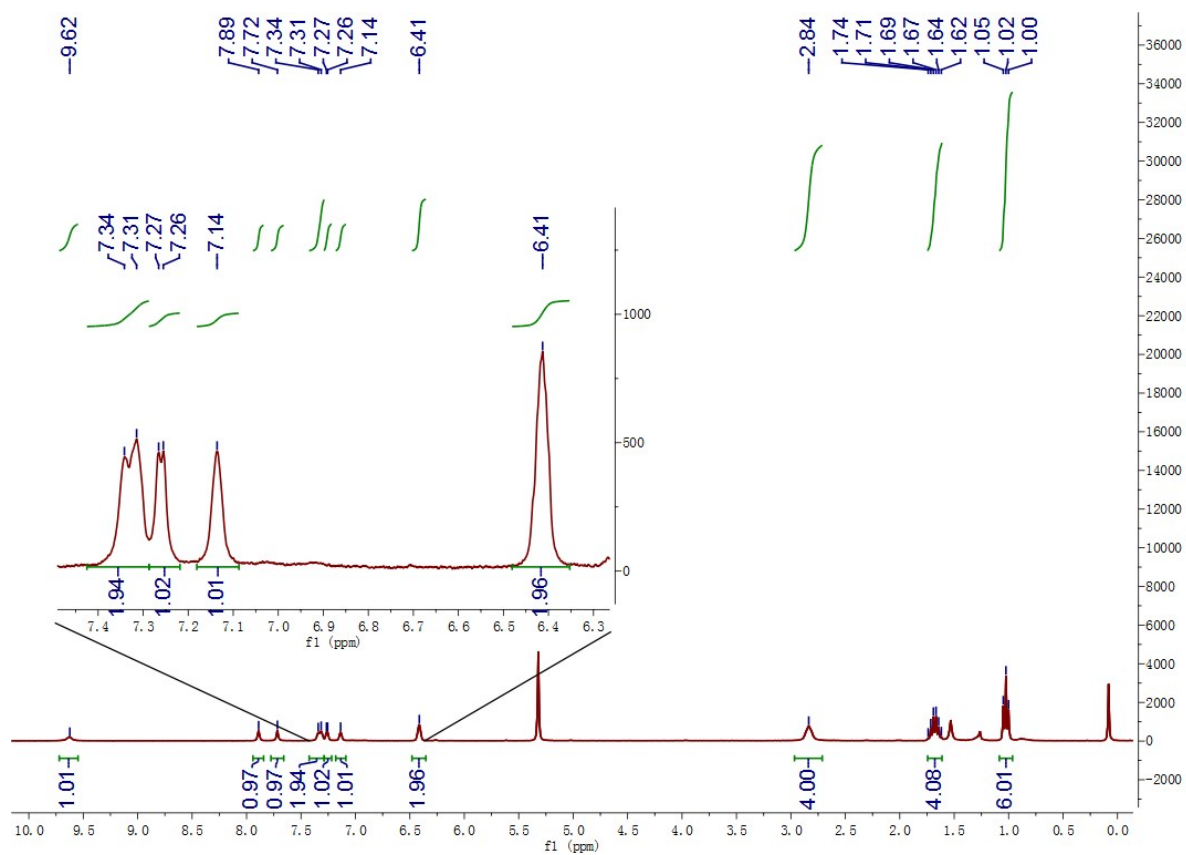
Synthesis of TTF-QB. To TTF-PQ (58 mg, 0.1 mmol) in toluene (10 mL) was added 1,8-diazabicyclo [5.4.0] undec-7-ene (DBU) (0.2 mL, 1.3 mmol). The mixture was refluxed for 10 min, and boron trifluoride diethyl etherate (0.24 mL, 1.9 mmol) was added into the reaction mixture. The reaction mixture was refluxed for 4 h, cooled down to room temperature and solvent was removed under vacuum. The crude product was purified by silica gel column chromatography (hexane/dichloromethane = 1:1, v/v). The product was obtained as a dark-blue powder in 60% yield (38 mg). ¹H NMR δ 9.62 (s, 1H), 7.89 (s, 1H), 7.72 (s, 1H), 7.42-7.29 (m, 2H), 7.26 (d, *J* = 3.1 Hz, 1H), 7.18-7.08 (m, 1H), 6.48-6.35 (m, 2H), 2.97-2.71 (m,

4H), 1.76-1.60 (m, 4H), 1.02 (t, $J = 7.3$ Hz, 6H). HR-MS (ESI, positive): m/z calcd for $C_{26}H_{23}N_4BF_2S_6$ 632.0303, found 632.0294. Elemental analysis (%) calcd for $C_{26}H_{23}N_4BF_2S_6$: C, 49.36; H, 3.66; N, 8.86; found: C, 49.34; H, 3.62; N, 8.71.

Synthesis of PQ. The compound was prepared according to the modified literature procedure.² A mixture of *o*-phenylenediamine (54 mg, 0.5 mmol) and 1,2-di(1*H*-2-pyrrolyl)-ethane-1,2-dione (47 mg, 0.25 mmol) in toluene (10 mL) and a catalytic amount of HOAc (0.1 mL) was refluxed for 8 h under nitrogen and cooled down to room temperature. The solvent was removed under vacuum and the crude product was purified by column chromatography (silica gel, hexane/dichloromethane = 1:1, v/v) to give the compound PQ (50 mg, 77%) as a purple-red solid. 1H NMR δ 9.70 (s, 2H), 7.91 (dd, $J = 6.3$ Hz, $J = 3.5$ Hz, 2H), 7.61 (2 \times d, $J = 6.4$ Hz, 2H), 7.04-7.02 (m, 2H), 6.93-6.90 (m, 2H), 6.28-6.25 (m, 2H).

Synthesis of QB. The compound was prepared according to the modified literature procedure.² To PQ (35 mg, 0.134 mmol) in toluene (10 mL) was added 1,8-diazabicyclo [5.4.0] undec-7-ene (DBU) (0.26 mL, 1.74 mmol). The mixture was refluxed for 10 min, and boron trifluoride diethyl etherate (0.31 mL, 2.54 mmol) was added into the reaction mixture. The reaction mixture was refluxed for 4 h, cooled down to room temperature and solvent was removed under vacuum. The crude product was purified by column chromatography (silica gel, hexane/dichloromethane = 1:1, v/v). The compound was obtained as a dark-blue powder in 68% yield (28 mg). 1H NMR δ 9.72 (s, 1H), 8.17 – 8.05 (m, 1H), 8.03 – 7.97 (m, 1H), 7.78 – 7.62 (m, 2H), 7.39-7.35 (m, 2H), 7.32 (d, $J = 3.8$ Hz, 1H), 7.17 (m, 1H), 6.45-6.41 (m, 2H).

¹H NMR spectrum of TTF-QB (CD₂Cl₂, 300 MHz)



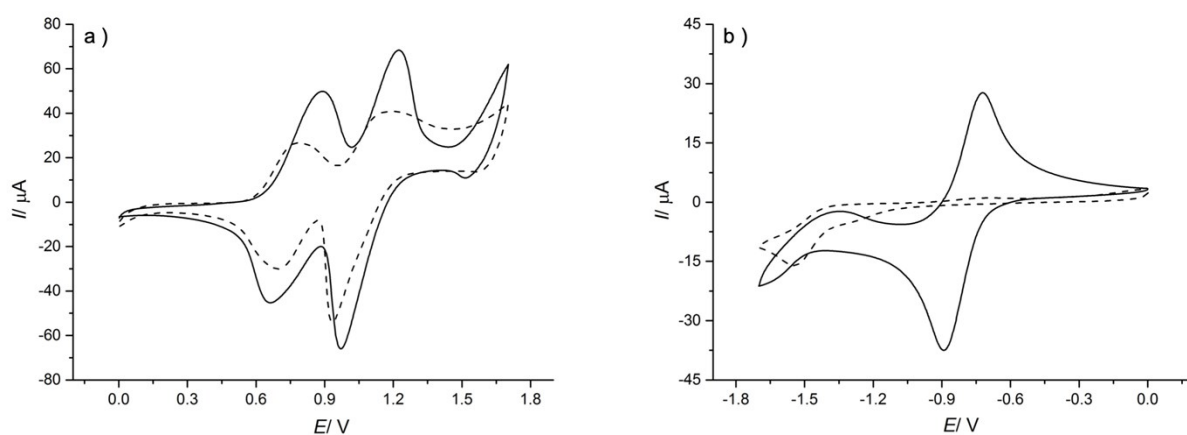


Figure S1 Cyclic voltammograms of TTF-QB (solid line) and TTF-PQ (dashed line) were measured in dichloromethane solution, containing 0.1 M TBAPF₆ as the supporting electrolyte at room temperature, Pt working electrode, Ag/AgCl electrode as the reference electrode and the scan rate at 100 mV s⁻¹.

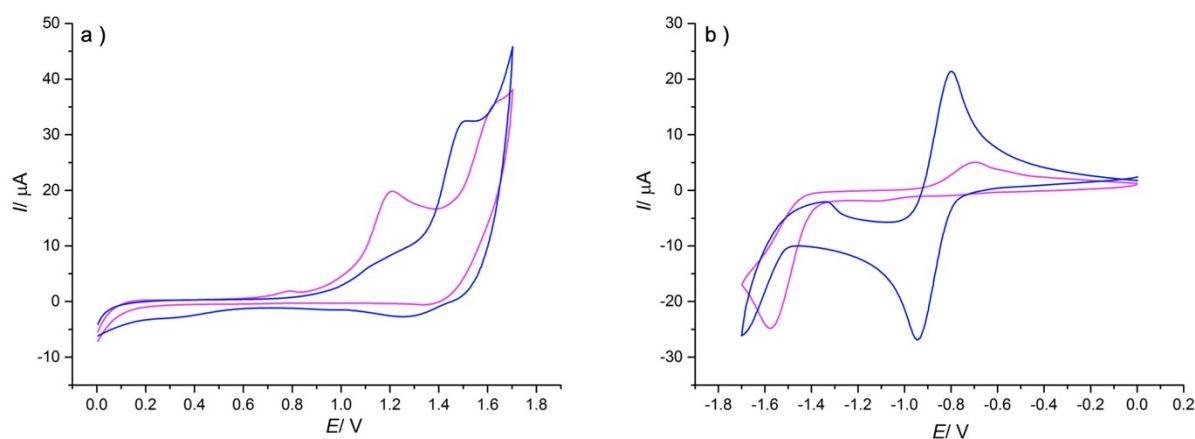


Figure S2 Cyclic voltammograms of QB (blue) and PQ (pink) were measured in dichloromethane solution, containing 0.1 M TBAPF₆ as the supporting electrolyte at room temperature, a platinum electrode as a working electrode, Ag/AgCl electrode as the reference electrode and the scan rate at 100 mV s⁻¹.

Table S1 Electrochemical data. Redox potentials [V] vs. Ag/AgCl in CH₂Cl₂.

Compound	$E_{1/2}^{\text{ox}1}$ (V)	$E_{1/2}^{\text{ox}2}$ (V)	$E_{1/2}^{\text{red}1}$ (V)	HOMO (eV)	LUMO (eV)	E_g (eV)	Optical gap (eV)
TTF-QB	0.78	1.10	-0.81	-4.96	-3.59	1.37	1.69
TTF-PQ	0.74	1.01 ^b	-1.55 ^a	-4.91	-3.00	1.91	2.23
QB	1.51 ^a		-0.88	-5.60	-3.51	2.09	2.25
PQ	1.21 ^a		-1.58 ^a	-5.34	-2.90	2.44	2.71

^a Irreversible process; ^b quasi-reversible process. $E_{\text{LUMO}} = -e (E_{\text{red}}^{\text{onset}} + 4.31)$, $E_{\text{HOMO}} = -e (E_{\text{ox}}^{\text{onset}} + 4.31)$, $E_{\text{red}}^{\text{onset}}$ = the onset reduction potentials, $E_{\text{ox}}^{\text{onset}}$ = the onset oxidation potentials, $E_{\text{HOMO}} = E_{\text{LUMO}} - E_{\text{g}}$, optical gap = $1240/\lambda_{\text{onset}}$. Fc/Fc⁺ is 0.49 V relative to Ag/AgCl in CH₂Cl₂.

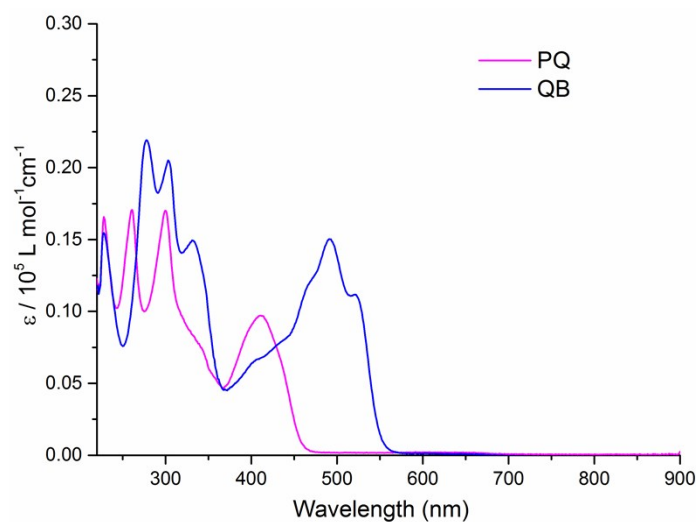


Fig. S3 UV-Vis spectra of PQ and QB (1.6×10^{-5} M) in CH₂Cl₂ at room temperature.

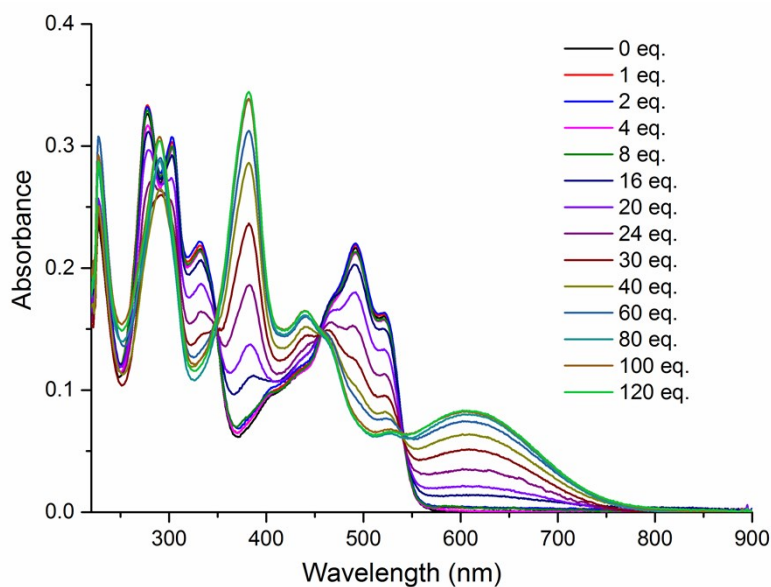


Fig. S4 Evolution of the UV-vis spectra of QB (1.5×10^{-5} M in CH₂Cl₂) during titration with tetrabutylammonium fluoride trihydrate (TBAF).

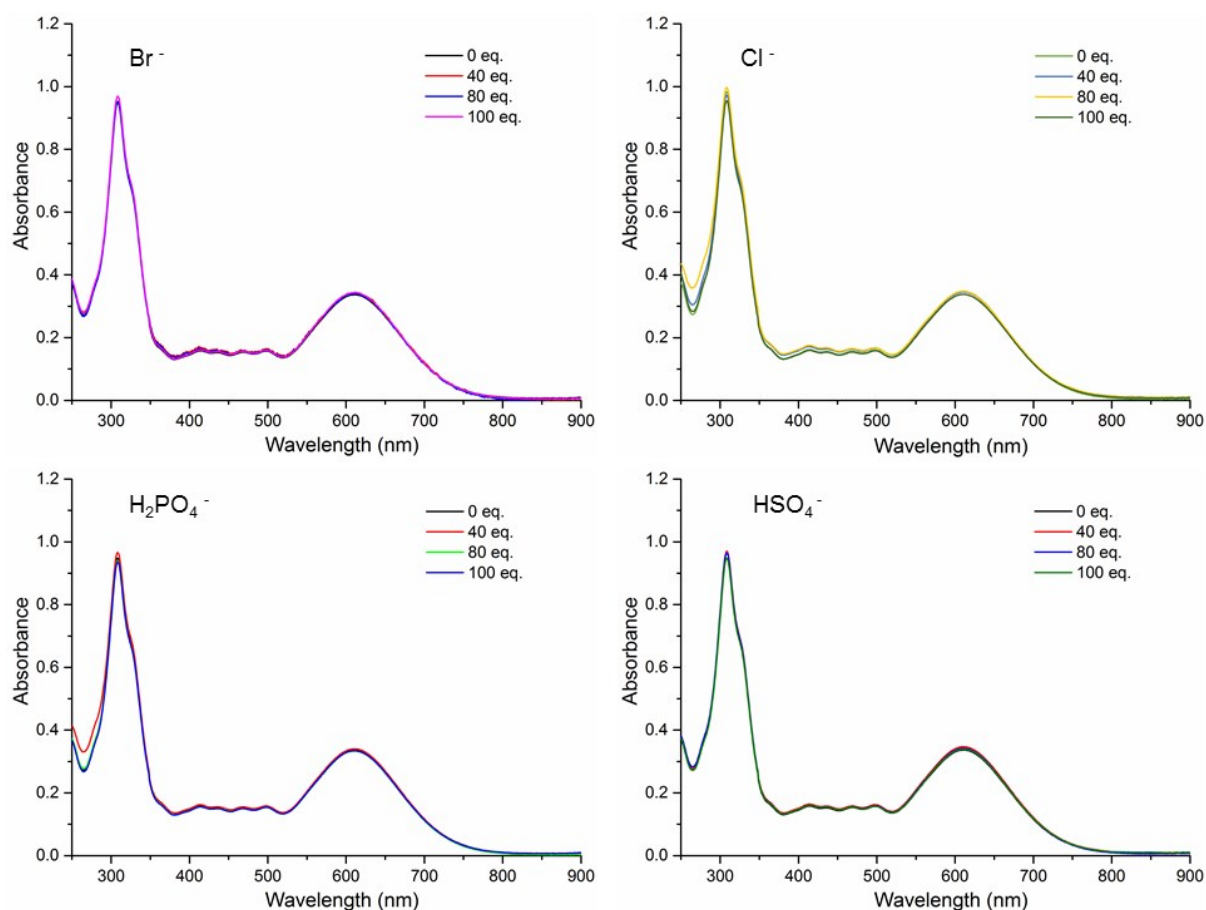


Figure S5 UV-vis spectral changes of TTF-QB upon the addition of anions Br⁻, Cl⁻, H₂PO₄⁻ and HSO₄⁻ (with their tetrabutylammonium salts) in CH₂Cl₂, 25 °C.

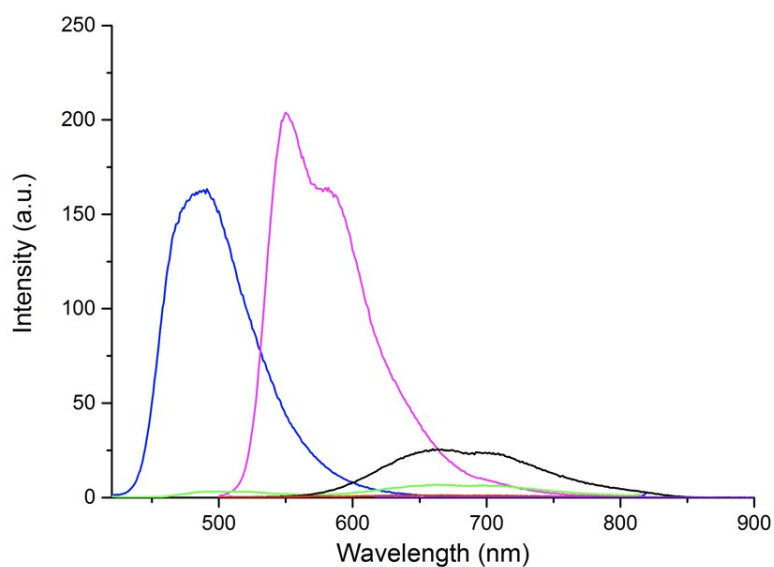


Figure S6 Fluorescent emission spectra of PQ (blue, λ_{ex} = 410 nm), QB (pink, λ_{ex} = 490 nm), TTF-PQ (green, λ_{ex} = 410 nm; black, λ_{ex} = 490 nm) and TTF-QB (red, λ_{ex} = 490 nm; purple, λ_{ex} = 610 nm) recorded in CH₂Cl₂ at room temperature and concentrations are 3.2×10^{-6} M.

The emission spectra of PQ, QB, TTF-PQ and TTF-QB were recorded in CH_2Cl_2 at room temperature under identical conditions as shown in Fig. 2. Upon excitation at 410 nm, compound PQ shows a strong emission centred at 490 nm while QB emission was red-shifted to 550 nm with a shoulder at 582 nm upon excitation at 490 nm, very probably due to extended π -conjugation upon complexation with BF_2 unit. Fluorescence emission from photo-excited PQ or QB is completely quenched by introduction of an electron donor TTF unit. Upon excitation at 490 nm, TTF-PQ shows a weak emission at 664 nm, stemming from the ICT transition. TTF-QB is non-emissive.

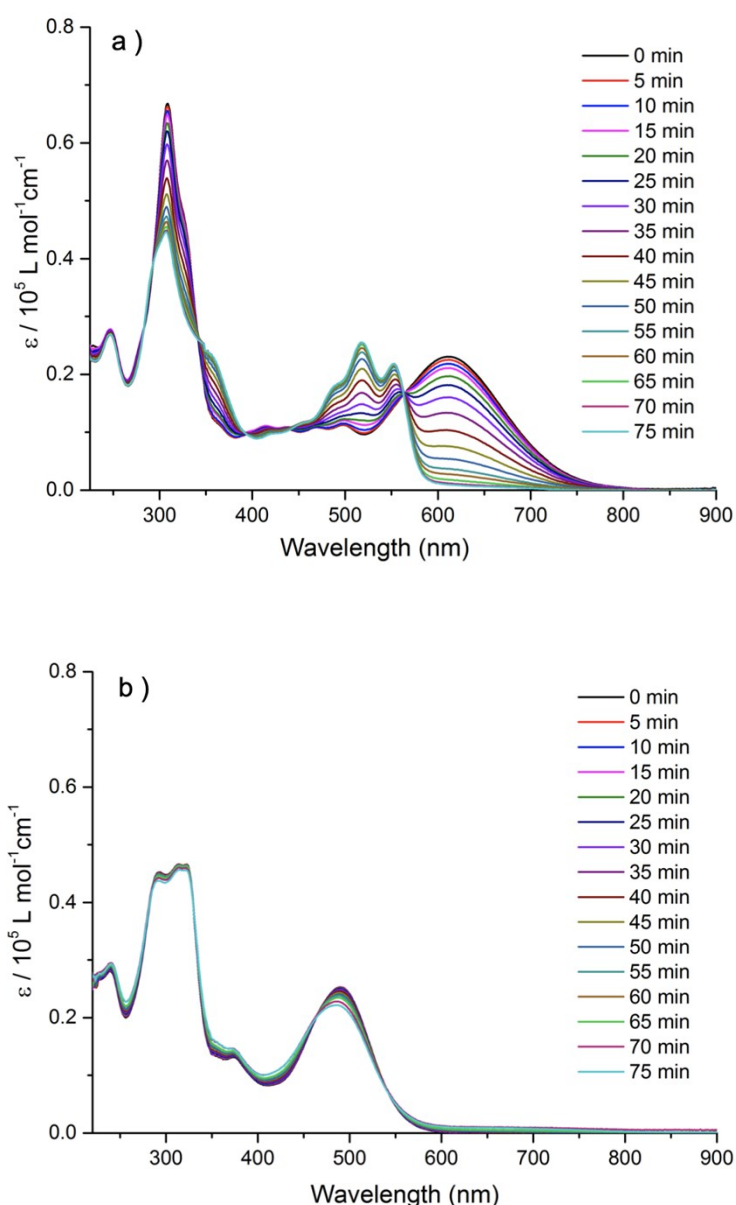


Figure S7 Changes in UV-Vis absorption spectra of TTF-QB (a) and TTF-PQ (b) as a function of time under daylight irradiation until the photostationary state is reached at a concentration of $1.6 \times 10^{-5} \text{ M}$ in CH_2Cl_2 .

The light-induced response of TTF-QB was monitored by UV-vis absorption spectroscopy in CH_2Cl_2 at room temperature (Fig. S7a). Upon daylight irradiation, an increase in the absorption range from 440 nm to 560 nm was observed, along with a decrease in the absorption maximum at 300 nm and a complete disappearance of the ICT band at 610 nm. Accordingly, the solution color changed from blue to pink (Fig. S8). In addition, clear isosbestic points at 342, 394, 440 and 563 nm were observed, indicating a full conversion of TTF-QB to a new species characterized by distinct absorption features. The absorption spectra of TTF-PQ, QB and PQ were measured under the same condition as control experiments (Fig. S7b, Fig. S9 and Fig. S10). In contrast, only a negligible spectral change of both TTF-PQ and QB was observed. All these results suggest that the BF_2 complexation facilitates photochemical transformation of TTF-QB which must happen at the TTF moiety. Based on the previously reported results,³ an oxidative cleavage of the central C=C bond occurs leading to the complete transformation of TTF-QB to **1** and **2**, as shown in Scheme S2. Moreover, a noticeable spectral variation of PQ is most likely due to the polymerization of the pyrrole groups.



Figure S8 Color changes of TTF-QB solution observed under daylight irradiation lasting 75 min.

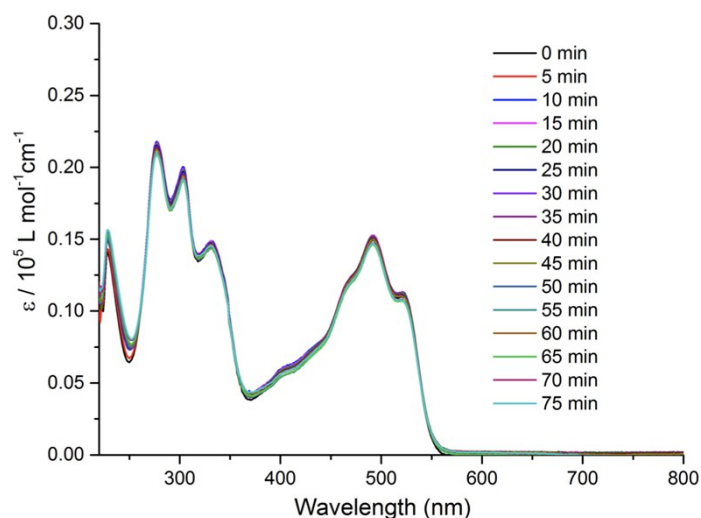


Figure S9 Changes in UV-Vis absorption spectra of QB (1.6×10^{-5} M in CH_2Cl_2) under daylight irradiation with different time until the photostationary state.

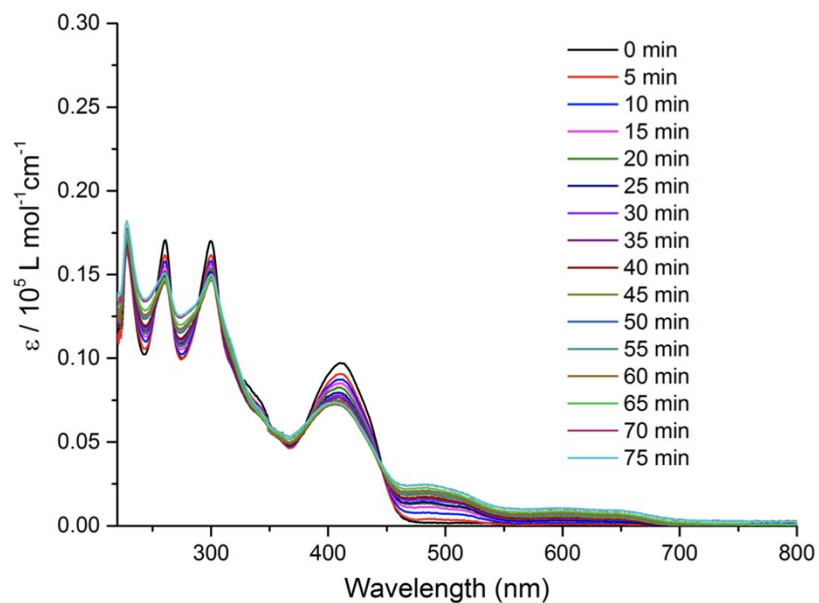
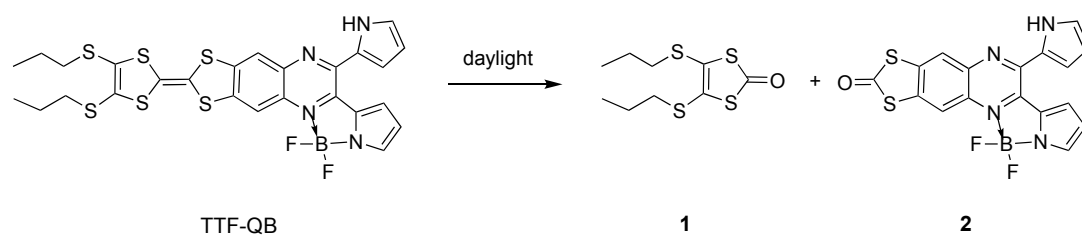


Figure S10 Changes in UV-Vis absorption spectra of PQ (1.6×10^{-5} M in CH_2Cl_2) under daylight irradiation with different time until the photostationary state is reached.



Scheme S2. A photochemical reaction of TTF-QB.

Table S2 Values of energies, oscillator strengths and dominant contributions of the respective molecular orbitals for $S_0 \rightarrow S_n$ of TTF-QB.

State	Wavelength (nm)	Oscillator strength	Major contributions	Minor contributions
S_1	617.45116	0.3516	HOMO->LUMO (99%)	
S_2	474.417208	0.1933	HOMO-1->LUMO (96%)	HOMO-2->LUMO+1 (2%)
S_3	430.231775	0.0241	HOMO-2->LUMO (98%)	
S_4	424.719762	0.0002	HOMO->LUMO+2 (95%)	HOMO-1->LUMO+2 (3%)
S_5	401.035687	0.0575	HOMO->LUMO+1 (95%)	
S_6	365.174932	0.0207	HOMO-5->LUMO (58%) HOMO-4->LUMO (12%) HOMO-3->LUMO (23%)	HOMO-1->LUMO+1 (4%)
S_7	359.239107	0.0016	HOMO-4->LUMO (70%)	HOMO-6->LUMO (9%) HOMO-5->LUMO (9%) HOMO-1->LUMO+1 (9%)
S_8	358.211583	0.0013	HOMO-5->LUMO (19%) HOMO-3->LUMO (70%)	HOMO-6->LUMO (5%) HOMO-4->LUMO (3%)
S_9	351.230009	0.0098	HOMO->LUMO+3 (77%)	HOMO-6->LUMO (9%) HOMO-5->LUMO (3%) HOMO-4->LUMO (3%) HOMO-1->LUMO+1 (2%)
S_{10}	348.877801	0.0056	HOMO-6->LUMO (48%) HOMO-4->LUMO (11%) HOMO-1->LUMO+1 (14%) HOMO->LUMO+3 (16%)	HOMO-5->LUMO (2%) HOMO-3->LUMO (5%)
S_{11}	336.346897	0.0103	HOMO-7->LUMO (87%)	HOMO-6->LUMO (6%)
S_{12}	331.579464	0.2594	HOMO-6->LUMO (20%) HOMO-1->LUMO+1 (67%)	HOMO-7->LUMO (4%) HOMO-5->LUMO (4%)
S_{16}	305.011668	0.3851	HOMO-8->LUMO (42%) HOMO-2->LUMO+1 (33%) HOMO->LUMO+5 (10%)	HOMO-6->LUMO+1 (4%) HOMO-1->LUMO+2 (3%)
S_{17}	303.169486	0.8038	HOMO-8->LUMO (38%) HOMO-2->LUMO+1 (20%) HOMO-1->LUMO+2 (10%) HOMO->LUMO+5 (15%)	HOMO-7->LUMO (3%) HOMO->LUMO+4 (6%) HOMO->LUMO+7 (2%)

Table S3 Selected frontier molecular orbitals of TTF-QB.

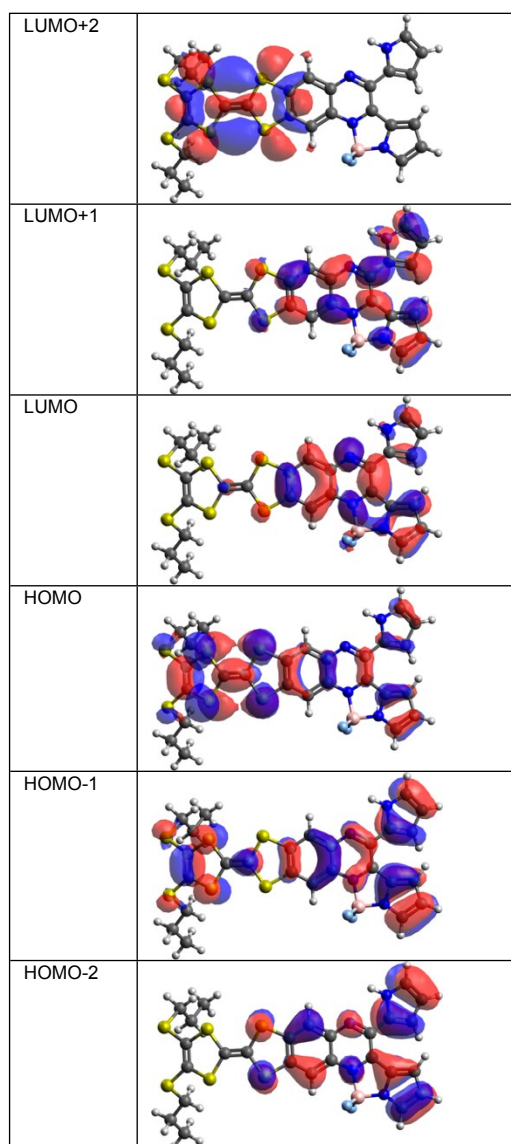


Table S4 Values of energies, oscillator strengths and dominant contributions of the respective molecular orbitals for $S_0 \rightarrow S_n$ of the fluoride adduct of TTF-QB.

State	Wavelength (nm)	Oscillator strength	Major contributions	Minor contributions
S_1	688.4568439	0.1439	HOMO->LUMO (96%)	HOMO->LUMO+3 (3%)
S_2	514.6280633	0.0087	HOMO->LUMO+1 (15%) HOMO->LUMO+2 (81%)	
S_3	503.5913607	0.0045	HOMO->LUMO+1 (82%) HOMO->LUMO+2 (15%)	
S_4	496.6320569	0.0001	HOMO-1->LUMO (97%)	
S_5	434.6509834	0.3249	HOMO-2->LUMO (93%)	
S_6	409.2427813	0.0021	HOMO-4->LUMO (61%) HOMO-2->LUMO+2 (19%)	HOMO-9->LUMO (3%) HOMO-5->LUMO (5%) HOMO-3->LUMO (4%) HOMO-3->LUMO+2 (3%)
S_7	406.3190438	0.0144	HOMO-4->LUMO (21%) HOMO-3->LUMO+2 (10%) HOMO-2->LUMO+2 (53%)	HOMO-2->LUMO (5%) HOMO-2->LUMO+1 (4%)
S_8	390.1450424	0.2078	HOMO->LUMO+3 (37%) HOMO->LUMO+4 (58%)	
S_9	385.4510757	0.0918	HOMO-3->LUMO (12%) HOMO-2->LUMO+1 (52%) HOMO->LUMO+4 (13%)	HOMO-3->LUMO+1 (6%) HOMO-2->LUMO+2 (6%) HOMO->LUMO+3 (6%)
S_{10}	385.1756594	0.1417	HOMO-3->LUMO (31%) HOMO-2->LUMO+1 (28%) HOMO->LUMO+3 (21%) HOMO->LUMO+4 (12%)	HOMO-3->LUMO+1 (3%)
S_{11}	372.8175157	0.0927	HOMO-5->LUMO (53%) HOMO-3->LUMO (23%)	HOMO-4->LUMO (9%) HOMO->LUMO+3 (7%) HOMO->LUMO+4 (5%)
S_{12}	369.9916234	0.2391	HOMO-5->LUMO (35%) HOMO-3->LUMO (27%) HOMO->LUMO+3 (21%)	HOMO->LUMO+4 (9%)
S_{22}	317.5824616	0.1033	HOMO-9->LUMO (10%) HOMO-8->LUMO (60%) HOMO->LUMO+8 (11%)	HOMO-7->LUMO (6%)
S_{28}	302.2677678	0.3338	HOMO-2->LUMO+3 (39%) HOMO-2->LUMO+4 (27%)	HOMO-7->LUMO (3%) HOMO-4->LUMO+1 (8%) HOMO-2->LUMO+6 (3%) HOMO->LUMO+9 (8%)

Table S5 Selected frontier molecular orbitals of the fluoride adduct of TTF-QB.

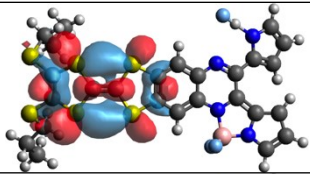
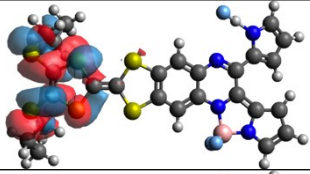
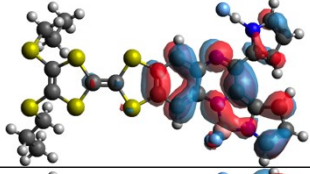
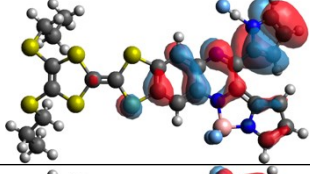
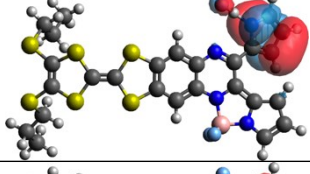
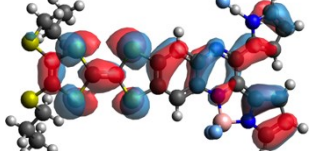
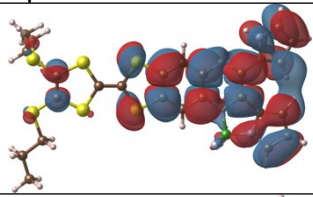
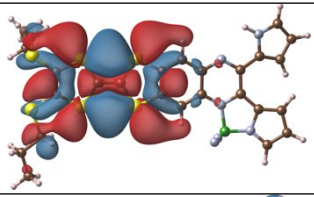
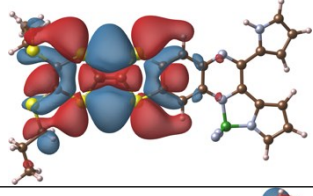
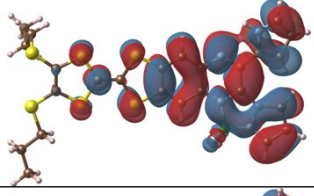
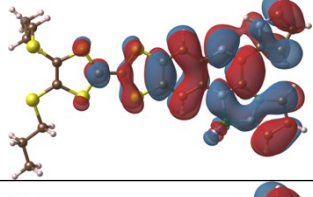
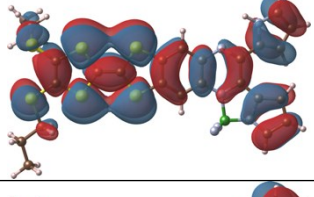
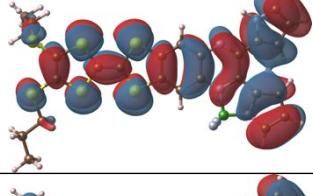
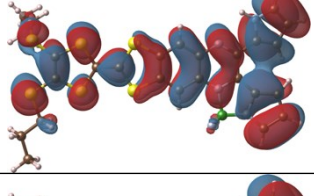
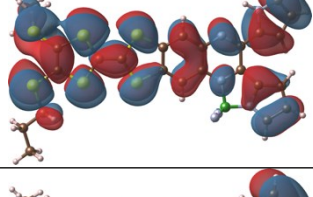
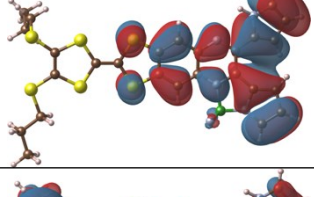
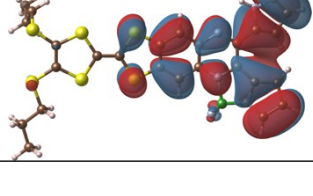
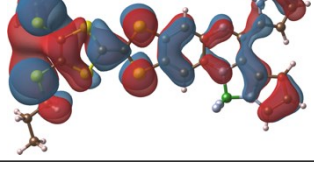
LUMO+2	
LUMO+1	
LUMO	
HOMO	
HOMO-1	
HOMO-2	

Table S6 Values of energies and dominant contributions of the respective molecular orbitals for $D_0 \rightarrow D_n$ of the radical cation of TTF-QB.

State	Wavelength (nm)	Major contributions	Minor contributions
D_1	1483.06451	HOMO(B)->LUMO(B) (98%)	HOMO(A)->LUMO(A) (3%)
D_2	1074.57266	HOMO-1(B)->LUMO(B) (97%)	
D_3	816.115015	HOMO-2(B)->LUMO(B) (89%)	HOMO(A)->LUMO(A) (7%)
D_4	740.911874	HOMO(A)->LUMO(A) (35%) HOMO(B)->LUMO+1(B) (42%)	HOMO-1(A)->LUMO(A) (7%) HOMO-2(B)->LUMO(B) (8%) HOMO(B)->LUMO(B) (3%)
D_5	665.222626	HOMO-3(B)->LUMO(B) (92%)	HOMO-5(B)->LUMO(B) (2%) HOMO-3(B)->LUMO+1(B) (2%)
D_6	647.707622	HOMO-5(B)->LUMO(B) (93%)	HOMO-4(B)->LUMO(B) (2%)
D_7	611.663508	HOMO-2(A)->LUMO(A) (17%) HOMO-6(B)->LUMO(B) (13%) HOMO-4(B)->LUMO(B) (38%) HOMO-1(B)->LUMO+1(B) (19%)	HOMO(A)->LUMO+2(A) (3%) HOMO-5(B)->LUMO(B) (2%)
D_8	602.069601	HOMO-2(A)->LUMO(A) (10%) HOMO-6(B)->LUMO(B) (17%) HOMO-4(B)->LUMO(B) (56%) HOMO-1(B)->LUMO+1(B) (11%)	HOMO(A)->LUMO+2(A) (2%)
D_9	567.953243	HOMO-6(B)->LUMO(B) (68%) HOMO-1(B)->LUMO+1(B) (14%)	HOMO-2(A)->LUMO(A) (9%) HOMO-1(B)->LUMO(B) (2%) HOMO(B)->LUMO+3(B) (2%)
D_{10}	525.245469	HOMO(A)->LUMO(A) (50%) HOMO(B)->LUMO+1(B) (35%)	HOMO-1(A)->LUMO(A) (6%)
D_{11}	498.78985	HOMO-1(A)->LUMO+1(A) (28%) HOMO(A)->LUMO+1(A) (68%)	
D_{12}	464.39506	HOMO-1(A)->LUMO(A) (67%) HOMO-8(B)->LUMO(B) (16%) HOMO(B)->LUMO+1(B) (12%)	
D_{13}	439.22415	HOMO-1(A)->LUMO(A) (10%) HOMO-8(B)->LUMO(B) (66%)	HOMO-2(A)->LUMO(A) (5%) HOMO(A)->LUMO+3(A) (2%) HOMO-1(B)->LUMO+1(B) (7%) HOMO(B)->LUMO+1(B) (2%)
D_{14}	435.169678	HOMO-7(B)->LUMO(B) (95%)	HOMO-1(B)->LUMO+1(B) (2%)
D_{15}	434.027141	HOMO-2(A)->LUMO(A) (49%) HOMO(A)->LUMO+2(A) (10%) HOMO-1(B)->LUMO+1(B) (23%)	HOMO-4(A)->LUMO(A) (2%) HOMO-1(A)->LUMO(A) (2%) HOMO-8(B)->LUMO(B) (6%)
D_{16}	430.635244	HOMO(A)->LUMO+2(A) (29%) HOMO-1(B)->LUMO+1(B) (14%) HOMO(B)->LUMO+2(B) (25%) HOMO(B)->LUMO+3(B) (22%)	HOMO-8(B)->LUMO(B) (2%)
D_{17}	429.799262	HOMO(A)->LUMO+2(A) (11%) HOMO(B)->LUMO+2(B) (71%)	HOMO-1(B)->LUMO+1(B) (5%) HOMO(B)->LUMO+3(B) (8%)
D_{18}	423.298713	HOMO-4(A)->LUMO(A) (35%) HOMO-3(B)->LUMO+1(B) (35%)	HOMO-4(A)->LUMO+2(A) (3%) HOMO-3(A)->LUMO(A) (5%) HOMO(A)->LUMO+2(A) (4%) HOMO-3(B)->LUMO(B) (3%) HOMO-3(B)->LUMO+3(B) (3%)

As TD-DFT calculations of open-shell systems tend to be affected by spin contamination,⁴ we do not give the oscillator strengths, that may be wrongly computed, and only consider transitions that can be associated to specific molecular orbitals with a very high proportion.

Table S7 Selected frontier molecular orbitals of the radical cation of TTF-QB.

MO	Alpha	Beta
LUMO+2		
LUMO+1		
LUMO		
HOMO		
HOMO-1		
HOMO-2		

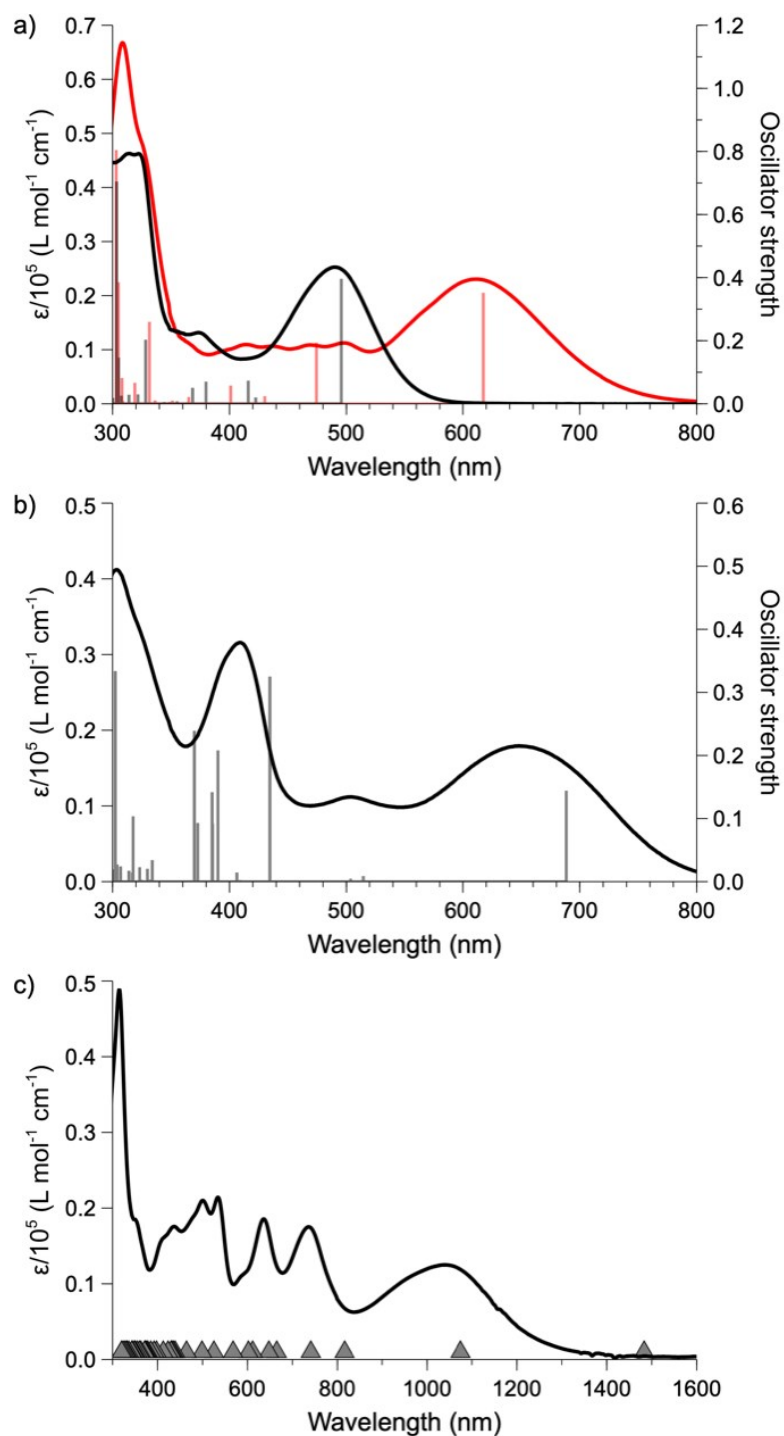


Figure S11 Absorption spectra of TTF-PQ (a, black), TTF-QB (a, red), its fluoride adduct (b) and radical cation species (c) together with their vertical electronic transitions. Please note that in (c) for the TTF^{•+}-QB, only excitation energies are given with trigonal symbols whereas oscillator strengths are omitted as aforementioned.⁴

References

1. H.-P. Jia, J. C. Forgie, S.-X. Liu, L. Sanguinet, E. Levillain, F. Le Derf, M. Salle, A. Neels, P. J. Skabara and S. Decurtins, *Tetrahedron*, 2012, **68**, 1590.
2. C. Yu, E. Hao, T. Li, J. Wang, W. Sheng, Y. Wei, X. Mu and L. Jiao, *Dalton Trans*, 2015, **44**, 13897.
3. L. K. Keniley, N. Dupont, L. Ray, J. Ding, K. Kovnir, J. M. Hoyt, A. Hauser and M. Shatruk, *Inorg. Chem.*, 2013, **52**, 8040; A. Charlton, D. Donati, S. Fusi, P. J. Murphy and F. Ponticelli, *Tetrahedron Lett.*, 2013, **54**, 1227.
4. Z. Li and W. Liu, *J. Chem. Theory Comput.*, 2016, **12**, 238.